Carrier-Phase Time Transfer

Kristine M. Larson and Judah Levine

Abstract—**We have conducted several time-transfer experiments using the phase of the GPS carrier rather than the code, as is done in current GPS-based time-transfer systems. Atomic clocks were connected to geodetic GPS receivers; we then used the GPS carrier-phase observations to estimate relative clock behavior at 6-minute intervals. GPS carrier-phase time transfer is more than an order of magnitude more precise than GPS common view time transfer and agrees, within the experimental uncertainty, with two-way satellite time-transfer measurements for a 2400-km baseline. GPS carrier-phase time transfer has a stability of 100 ps, which translates into a frequency uncertainty of about two parts in 10^{15} for an average time of 1 d.**

I. Introduction

GPS in the precise time-transfer community has been dominated by the common view technique, which uses the C/A pseudorange observable and explicit differencing of the GPS data collected at the two timing observatories [1]. Observatories using single-channel, single-frequency C/A code receivers routinely report accuracies of a few nanoseconds for a standard 13-minute pass and a frequency uncertainty on the order of two parts in 10^{14} over one day. Single frequency multi-channel receivers have also been used for common view analysis; recent results suggest that these receivers are capable of 2.5-ns RMS over short baselines and 5 ns or better over baselines of 2400 km in length [2].

In the geophysical communities where geologic deformation rates are often on the order of 1 mm/yr, the pseudorange observable is not sufficiently precise [3]. Therefore, geophysicists use geodetic GPS receivers that measure the phase of the carrier as well as the pseudorange; they have obtained position estimates with uncertainties of about 1 cm using these techniques and averaging the results for 1 day [4]. Because clocks and positions are both inherently related to the GPS carrier-phase observable, it seems likely that GPS carrier-phase techniques can also be used for accurate time transfer.

The potential of GPS carrier phase for time transfer has been recognized and described by others. A group at JPL suggested that the carrier-phase technique was capable of estimating subnanosecond biases between hydrogen masers at continental scales [5]. Several years later, additional analysis from the same group reported Allan deviations between masers ranging from four to nine parts in 10^{15} for averaging times between 10^4 and 10^5 seconds [6]. A group in Switzerland has also pioneered use of the carrier-phase technique, suggesting 20-ps time transfer can be achieved over distances of several meters [7]–[10].

In this paper, we describe a series of experiments that we have conducted to test GPS carrier-phase techniques for high precision time transfer [11], [12]. An important aspect of our analyses is that we compared the results we obtained using carrier-phase methods with other independent estimates of the performance of the clocks that were connected to the receivers.

Manuscript received September 2, 1998; accepted December 16, 1998.

K. M. Larson is with JILA and Department of Aerospace Engineering Sciences, University of Colorado, Boulder, CO 80309.

J. Levine is with JILA and Time and Frequency Division, National Institute of Standards and Technology, Boulder, CO 80303.

II. The GPS-Phase Observable

The local oscillator connected to the GPS receiver is explicitly included in the carrier-phase model equation. The satellite-generated phase ϕ^s and the receiver-generated phase ϕ_r can be defined as a function of time t:

$$\phi^s(t) = f^s t - f^s \frac{\rho_g}{c} - f^s \delta^s \tag{1}$$

and

$$\phi_r(t) = f_r t - f_r \delta_r \tag{2}$$

where f is either the transmitter or receiver oscillator frequency, c is the speed of light, and δ_r and δ^s are receiver and transmitter clock errors, respectively [13]. ρ_g is the geometric range or $|\vec{X}^s - \vec{X}_r|$, where $\vec{X}^s$ is the satellite position at the time the signal was transmitted from the satellite and $\vec{X}_r$ is the receiver position when the signal was received. Proper determination of ρ_g requires precise transformation parameters between the inertial and terrestrial reference frames, including models of precession, nutation, polar motion, and UT1-UTC.

The carrier-phase measurement $\phi_r^s(t)$ is the difference between the satellite-generated phase and the receiver-generated phase:

$$\begin{aligned} \phi_r^s(t) &= \phi^s(t) - \phi_r(t) \\ &= -f^s \frac{\rho_g}{c} - f^s \delta^s + f_r \delta_r + (f^s - f_r)t. \end{aligned} \tag{3}$$

f_r and f^s do not deviate significantly from the nominal GPS frequency f (1.575 42 GHz and 1.227 60 GHz for $L1$ and $L2$, respectively) which allows us to rewrite (3) as:

$$\phi_r^s(t) = -f \frac{\rho_g}{c} - f(\delta^s - \delta_r). \tag{4}$$

The GPS receiver only measures the phase modulo 2π $\Delta\phi_r^s(t)$; thus:

$$\phi_r^s(t) = \Delta\phi_r^s(t) + N_r^s = -f\frac{\rho_g}{c} - f(\delta^s - \delta_r) \qquad (5)$$

where N_r^s is the initial number of integer cycles, known as the carrier-phase ambiguity or bias. Multiplying (5) by the carrier wavelength λ, we can rewrite the observable equation as follows:

$$-\Delta\phi_r^s\lambda = \rho_g + c\delta^s - c\delta_r + N_r^s\lambda. \qquad (6)$$

Because the signal must travel through both the ionosphere and troposphere and given that some signals are reflected before they are received, the observable equations for $L1$ and $L2$ can be rewritten as:

$$\begin{aligned}\Phi_{1r}^s &= -\Delta\phi_{1r}^s\lambda_1 \\ &= \rho_g + c\delta^s - c\delta_r + N_{1r}^s\lambda_1 + \rho_t - \rho_{i1} + \rho_{m1} + \epsilon_1\end{aligned} \qquad (7)$$

$$\begin{aligned}\Phi_{2r}^s &= -\Delta\phi_{2r}^s\lambda_2 \\ &= \rho_g + c\delta^s - c\delta_r + N_{2r}^s\lambda_2 + \rho_t - \rho_{i2} + \rho_{m2} + \epsilon_2\end{aligned} \qquad (8)$$

where ρ_t and ρ_i are the propagation delays caused by the troposphere and ionosphere and ρ_m is the multipath error. ϵ represents unmodeled errors and receiver noise. Note that the contribution from the troposphere at the GPS frequencies is not frequency dependent, but the multipath, ionosphere, and random error terms are.

The ionospheric delay ρ_i varies to first order as 40.3 TEC/f^2, where TEC is the total electron content along the path between the receiver and satellite in units of electrons/meter^2, and the total delay is given in meters. We can combine the $L1$ and $L2$ observables to remove this frequency dependence, obtaining the ionosphere-free linear combination Φ_{cr}^s:

$$\Phi_{cr}^s = \frac{f_1^2}{f_1^2 - f_2^2}\Phi_{1r}^s - \frac{f_2^2}{f_1^2 - f_2^2}\Phi_{2r}^s \approx 2.55\Phi_{1r}^s - 1.55\Phi_{2r}^s. \qquad (9)$$

In terms of the model parameters, Φ_{cr}^s can be written as:

$$\Phi_{cr}^s = \rho_g + c\delta^s - c\delta_r + B_{cr}^s + \rho_t + \rho_{cm} + \epsilon_c \qquad (10)$$

where the new ambiguity term B_{cr}^s is:

$$B_{cr}^s = \frac{f_1^2\lambda_1 N_{1r}^s - f_2^2\lambda_2 N_{2r}^s}{f_1^2 - f_2^2} \qquad (11)$$

The benefit of the ionosphere-free combination is that a large systematic error is eliminated; the penalty comes from an increase in the random error. For a short baseline, it is acceptable to use either single-frequency data type; $L1$ is generally preferred because it has better signal to noise ratio and a shorter wavelength. To demonstrate this, we have computed two time-transfer solutions for a short baseline (less than 200 m). Hydrogen masers were connected to geodetic GPS receivers at each end of the baseline. In one case, we used only the $L1$ carrier-phase data, and, in the other, we used the ionosphere-free data combination of both frequencies. In Fig. 1, we show the two detrended differential clock solutions. The horizontal axis is the modified Julian date (MJD) in days. Although there are systematics in each time series that represent real clock noise and multipath, note that the short-term precision of the $L1$ solution is significantly better than that for the ionosphere-free solution (a TDEV of 5 ps vs. 13 ps for averaging times of 6 minutes). The RMS about the mean for either time series is 22 ps.

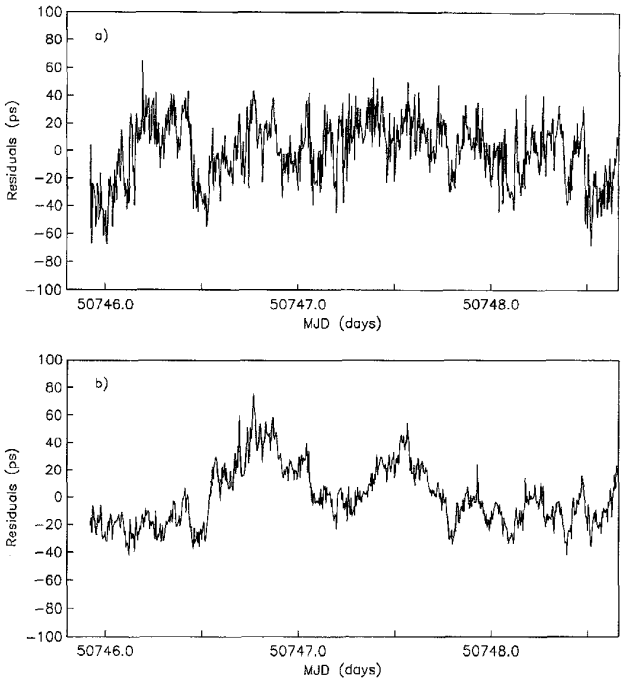

Fig. 1. Short baseline carrier-phase clock solutions using the ionosphere-free solution (upper panel) and the $L1$ data only (lower panel). Note the greater precision of the $L1$ data. Each data series has been detrended and is plotted about its mean.

If we denote the standard deviations for the $L1$ and $L2$ range equivalent carrier phases as σ_1 and σ_2 and if we assume that the $L1$ and $L2$ observations are not correlated, the random uncertainty for the ionosphere free combination, σ_{LC}, can be derived using standard propagation of errors:

$$\sigma_{LC}^2 = (2.55^2 \times \sigma_1^2) + (1.55^2 \times \sigma_2^2). \qquad (12)$$

The random uncertainty will then be approximately three times larger than the equivalent standard deviations for single frequency analysis. Because we are interested in time transfer at longer distances, for the remainder of this paper, we discuss only applications of the ionosphere free carrier-phase observable. The remaining parameters in (10), ρ_g, δ^s, δ_r, ρ_t, and B_{cr}^s, must be estimated or known a priori.

Similar equations can be derived for the pseudorange observable with a few important differences. The ionospheric correction is identical in magnitude but opposite in sign to that for the carrier-phase data. Pseudorange is an absolute observable; therefore, no bias/ambiguity term needs to be estimated. Most importantly, the range equivalent carrier-phase measurement is approximately 100 times more precise than typical pseudorange data.

III. Data Analysis

Equation (10) can be solved using standard least squares estimation techniques. We used a geodetic software, GIPSY, to analyze the GPS data [14]. GIPSY was developed to analyze carrier-phase GPS data to provide precise estimates of station coordinates. It also has fully developed capabilities to estimate the orbits of GPS satellites and other satellites with GPS receivers. GIPSY incorporates a modified sequential filter algorithm called a square root information filter (SRIF). The characteristics of this filter are described fully by [15], and we concentrate only on the time-varying parameters themselves rather than the algorithm. All time-varying "stochastic" parameters are modeled as a first-order Gauss-Markov process. The time-varying parameters are updated at the end of each time interval or "batch." In this analysis, we use two stochastic parameter formulations: a white noise model for the clocks and a random walk model for the troposphere delay. These kinds of stochastic models have also been used in analysis of data from very long baseline interferometers [16]. Both white noise and random walk parameterizations can be derived from the first-order Gauss-Markov process.

If $p(t)$ is the value of the stochastic parameter and $w(t)$ is the white process noise with zero mean value, then for a random walk process:

$$\frac{dp}{dt} = w(t) \tag{13}$$

and

$$p(t + \Delta t) = p(t) + w(t)\sqrt{\Delta t}. \tag{14}$$

We must specify a process noise variance to bound the random walk process. For a white noise process, we reset the variance for that parameter at each batch.

For our parameter estimates to have realistic uncertainties, we must decide how to weight the data. As we have defined the problem, we will be assuming that both the carrier-phase and pseudorange data can be represented as a white noise process. This means, for example, that we would expect a $\sqrt{N}$ improvement in precision as N, the number of observations, is increased. In practice, we find this is not true, and we find many different correlations in the residuals over short periods. Some of these correlations are due to an incomplete model of the observations, and other correlations are likely due to the measurements. In Fig. 2, we plot the carrier-phase residuals as a function of time after a model has been applied and all parameters have been estimated. (These are often called "post-fit residuals.") Although the post-fit residuals appear white when plotted as a function of time, we can demonstrate that they are not by plotting the residuals as a function of elevation angle. There is a slight broadening of the residuals at low elevation angles, which may reflect our inability to model the troposphere at low angles and greater impact of multipath reflections at these angles.

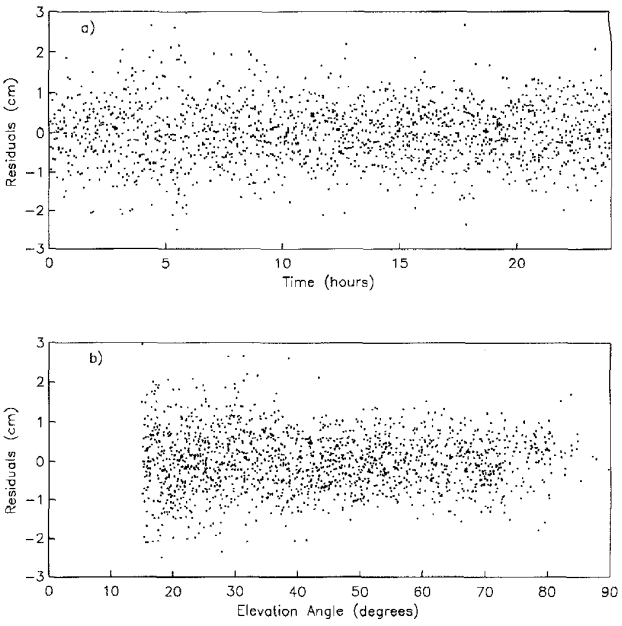

Fig. 2. Post-fit carrier-phase range residuals for the NIST receiver (connected to clock 16). The residuals are plotted as a function of time in the upper panel and as a function of elevation angle in the lower panel.

How do we choose a priori standard deviations for the observations? We could use the RMS of the carrier-phase residuals (as shown in Fig. 2) as the carrier-phase standard deviation and equivalently for the pseudorange observables. When we do so we find that the formal errors for estimated parameters (e.g., station coordinates) are too optimistic by about 50%. Therefore, we scale the data standard deviations, using 1 cm for carrier phase and 100 cm for pseudorange data. From analysis of many years of GPS carrier-phase and pseudorange data, we have found that these data weights provide more realistic formal errors for estimated parameters such as orbits [14] and station coordinates [17].

In Table I, we summarize the model input and the estimated parameters we used in this analysis. Both satellite and receiver clocks are estimated at each data epoch relative to a reference receiver clock, usually a receiver connected to a hydrogen maser. The clock behavior is modeled as white noise, so that the estimates are uncorrelated from epoch to epoch. In principle, high quality clocks, such as hydrogen masers, could be modeled as colored noise. In these experiments, we have not taken advantage of the

TABLE I
PARAMETERS USED IN THE DATA ANALYSIS

Model	Value/Reference	
Data interval	6 min	
Elevation angle cut-off	15°	
Geopotential	JGM3 degree and order 12	
Precession	IAU 1976 precession theory	
Nutation	IAU 1980 nutation theory	
Earth orientation	International Earth Rotation Service Bulletin B	
Yaw attitude	[18]	
Ephemerides	IGS precise orbits [19]	
Reference clock	NIST clock 16–hydrogen maser	
Pseudorange σ	100 cm	
Carrier-phase σ	1 cm	
Parameter	Estimation	Standard Deviation
Satellite clock	White noise	1 s
Station position, reference	Constant	1 cm
Station position, nonreference	Constant	1 km
Station clock	White noise	1 s
Phase ambiguity (real valued)	Constant	0.1 km
Zenith troposphere delay	Random walk	10 mm/square root(hour)

fact that we are using atomic clocks. We have set the variance for each clock parameter at each data epoch to 1 s^2. In doing so, we are assuming no a priori information, and we are assuming that the clock estimates are constrained only by the observations.

The satellite coordinates $\vec{X}^s$ are taken from the IGS service with a range accuracy of 5 to 10 cm [19]. The reported orbit accuracy varies, depending on whether the satellite is or is not in eclipse. Orbit accuracy is also affected somewhat by antispoofing, which degrades the pseudorange measurements and the $L2$ carrier-phase data. If a 10-cm orbit error is mapped directly into clock estimates, this would severely limit the value of carrier-phase data for time transfer. Fortunately, orbit errors project to a substantially smaller range error when one looks at relative quantities, such as relative station coordinates and differential clocks.

The troposphere varies both spatially and temporally. The question then becomes how much does it vary and how does that variation impact the accuracy of the observable model? Generally, the geodetic community has ignored the spatial complexities of the troposphere and has modeled the troposphere delay with a measurement or estimate of the delay at zenith. One then uses a mapping function to translate that zenith measurement to the current satellite elevation angle. Although a number of mapping functions has been published in the literature, they all vary to first order as the inverse sine of the elevation angle [20], [21]. The underlying assumption in this model is that the troposphere is azimuthally symmetric.

It is extremely important to model the zenith delay accurately. An error of 1 cm in the zenith delay produces over 5 cm of equivalent range error for a setting satellite as is shown in Fig. 3(a). This kind of error would significantly corrupt clock estimates. How much does the tropospheric zenith delay vary with time? This depends critically on the site and the weather. Some sites have very little variation throughout the day; others have variations in tens of centimeters. In Fig. 3(b), we have plotted the temporal variation of the zenith troposphere delay (minus a constant) for two sites. NIST, in Boulder, Colorado, has relatively little variation with time. Hawaii, on the other hand, has variations as large as 10 cm over a period of 4 h.

We can predict the zenith tropospheric delay by combining ground measurements of pressure, temperature, and humidity [22]. Unfortunately, this method is not sufficiently precise for geodetic purposes (nor for precise time transfer), primarily because the portion of the tropospheric delay caused by water vapor is difficult to predict from the ground. We can also estimate the zenith delay by using the GPS data themselves. Temporal variations of the zenith delay have been modeled in one of two ways. In the first technique, we assume that the zenith delay behaves linearly over some period of time, estimating a new parameter for the next time period that is consistent at the intersection point. We use the second technique in which the troposphere variation is estimated as a stochastic parameter. The assumption of azimuthal symmetry is discussed in [23]–[25].

Although the observable equations for carrier phase are straightforward in principle, carrier-phase data are more difficult to use in practice than are pseudorange data. The primary drawback to using carrier-phase data is cycle slips. When the receiver loses lock on the signal, a new value for $N1_r^s$ or $N2_r^s$ must be used. An important element of any carrier-phase software is its ability to check the carrier-phase data for these cycle slips. Failure to identify and/or repair cycle slips results in grossly inaccurate results. We use a cycle slip algorithm that inspects and repairs cycle slips for each frequency and satellite separately, before the

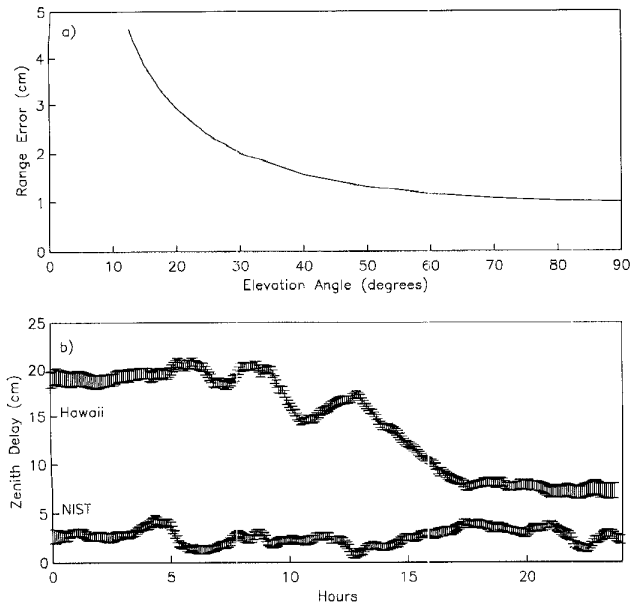

Fig. 3. a) Effect of a 1-cm error in the wet tropospheric zenith delay as a function of satellite elevation angle; b) estimated tropospheric zenith delays and one standard deviation uncertainties for sites in different troposphere regimes. The Hawaiian site is located on Kauai, and the NIST is located in Colorado. A large constant value has been removed from both series. Clearly, any assumption that the troposphere delay does not vary with time will result in large and systematic errors in the observable range model.

ionosphere-free data combination is formed [26].

Although the individual $N1_r^s$ and $N2_r^s$ ambiguities are integers, the ionosphere-free ambiguities are not. Therefore, Bc_r^s values for each satellite/station pair are estimated as real valued parameters. Algorithms have been developed to use the integer nature of the single frequency carrier-phase data after initial parameter estimation. Successful carrier-phase ambiguity resolution removes a large number of parameters from the estimation problem and strengthens the determination of the other parameters, including the receiver clocks [27].

On the other hand, algorithms that repair cycle slips can be fooled by a time step in the local clock. This ambiguity does not arise if the slip is only in the data from one satellite, but more complex situations involving several nearly simultaneous effects may not be handled correctly. This difficulty is discussed in greater detail in the next section.

IV. Geodetic GPS Receivers

Although the carrier-phase equations in the previous section are simple in principle, the internal design of a carrier-phase receiver adds a number of complications to the analysis that are not present for code-based time transfer. These differences are important because they are likely to impose important constraints on the accuracy of carrier-phase time transfer and, to a lesser extent, on carrier-phase frequency distribution. Some of these constraints may turn out to be unique to the receiver that we used, but the designer of any carrier-phase receiver must address these problems, and how they are addressed may have a significant impact on the usefulness of the receiver for time or frequency distribution.

The hardware design of a code-based time-transfer receiver is simple in concept. The pseudo-random codes that are used to modulate the GPS carrier contain natural time markers. Any receiver can extract this time marker by looking for the peak in the cross-correlation between the received code and a locally generated copy of it. The clock that generates the local copy of the code becomes locked to the GPS chipping frequency as a direct consequence of this cross-correlation process, and both its frequency and its phase are fully determined by the characteristics of the code. (The details of the cross-correlation process vary depending on whether the receiver is using the C/A code or the P code, but the result is the same in either case.) This relationship may be disturbed by transients or by a temporary loss of the signal, but both the frequency and the phase of the local clock are determined by the received code, and there cannot be any permanent offset in the data once the steady-state operation has resumed.

Once the local chipping clock is locked to the GPS signal, it is a straightforward matter to generate 1 pulse/s from this clock and to measure the difference between this signal and the corresponding output from a local reference. If the receiver is tracking more than one satellite, then this procedure will produce a measurement of the time difference between the local clock and GPS time using each satellite that is being tracked. Performing and reporting these different measurements add complications to a practical receiver, but the measurements remain unambiguous in principle.

The situation with carrier-phase measurements is more complicated, especially with a multichannel receiver that can track several satellites simultaneously. The first problem is that the received carrier and the local reference are not at the same frequency. The carrier frequency is much too high to be used to make phase measurements directly, and the details of how it is translated to a lower frequency by the front-end hardware are important because this translation will add phase shifts that will appear as time offsets in the output phase data. To make matters more complicated, each satellite has a different frequency because of Doppler shifts and similar effects, and these frequencies vary with time for the same reasons.

One way of dealing with this complexity is to use several down conversions with multiple local oscillators. The first one operates at a fixed frequency and is common to all of the channels in a multichannel receiver. It reduces the signals from all satellites to much lower frequencies using a single broadband mixer.

There is one copy of the second oscillator for each channel. (These multiple oscillators can be realized digitally using a single sine wave look-up table in read-only memory with a different pointer for each channel.) It is controlled

in frequency to track the Doppler shift of a single satellite. The overall phase shift added by this multiple conversion is the sum of the phase shifts, and all of them must be known for time-transfer measurements. Both of these phase shifts drop out in normal geodetic analyses—the first because it is common to all satellites in view and the second because it is known with very high accuracy. Neither of them is necessarily an integral number of carrier cycles; the exact values depend on the details of the receiver design.

These phase shifts do not limit the accuracy of carrier-phase frequency transfer in steady-state operation, but they may produce transients each time the receiver is started or when the receiver loses lock on a satellite. There may be a discontinuity in the carrier-phase data at these points. The value of the jump may not bear any simple relationship to the carrier period because the discontinuity may be related to the period of the intermediate frequencies that are internal to the receiver.

To make matters more complicated, a phase jump in a single channel is likely to be interpreted as a cycle slip by the postprocessing software. The software will "repair" this jump by adding or removing an integral number of carrier periods. This repair will probably leave a residual offset that will appear as clock noise. The magnitudes of these residual offsets will not be greater than one-half of a carrier period. If we assume that they are not correlated with the other contributions to the variance, then they contribute about 190 ps to the observed variance at periods comparable with the mean interval between them. This is not negligible, and, therefore, it is important to minimize the number of such resets by proper hardware design.

V. Results for Short Baselines

Over short baselines, geodetic parameters and clock data are insensitive to orbit error. This is also true of atmospheric conditions, which are common to both antennas for a short baseline. The limiting error sources in this case should be multipath, measurement noise, and clock noise.

We connected two geodetic quality GPS receivers [28] to NIST clock 16 and NIST clock 21. Clock 16 is a hydrogen maser, and clock 21 is a cesium standard. Each GPS antenna was mounted to the roof of the NIST facility. The distance between the antennas was 40 m. In Fig. 4(a), we have plotted the measurements of the time difference between clock 16 and clock 21 made using conventional (non-GPS) hardware. We will treat these measurements, made every 12 min, as "truth." In Fig. 4(b), we show the residual agreement (about the mean) between the GPS estimates and the truth standard using only the pseudorange data. The residuals show peak to peak scatter of nearly 10 ns, with a RMS agreement over the 7-d period of 2.3 ns. These estimates are comparable with what can be achieved using traditional common view techniques. In Fig. 4(c), we used the carrier-phase measurements (note the change in scale). The RMS of the carrier-phase residuals is 55 ps, nearly 50 times more precise than using pseudorange data. Both the pseudorange and carrier-phase residuals show variations with what appears to be a 24-hour period, which we think is associated with multipath reflections of the GPS signals. A pure multipath effect will produce identical residuals from day to day, advanced by 4 minutes to account for the orbital period. In practice, residuals will also reflect data quality and changes in the reflective characteristics of the nearby surfaces.

There may also be thermal effects in the data, but, because the antennas are in the same thermal environment, thermal effects would be evident only if the thermal sensitivities of the antennas were different. Because the antennas are the same model and from the same manufacturer, we expect these to be negligible. We know from other data

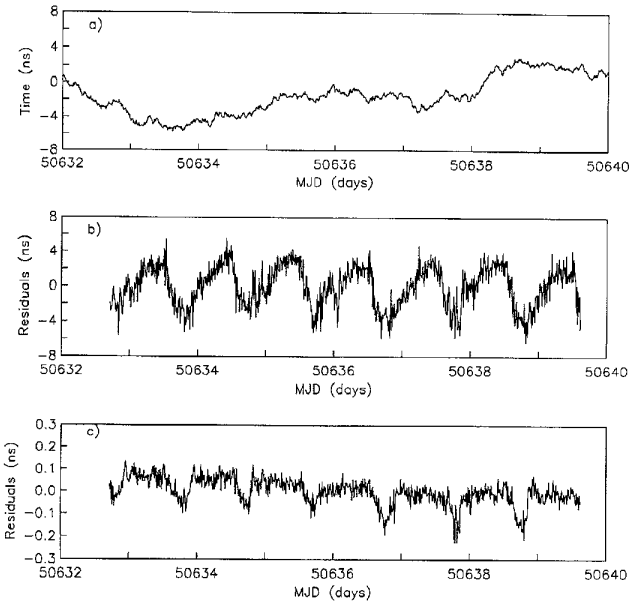

Fig. 4. a) Time difference between NIST clock 16 and clock 21 measured using conventional hardware; also, residuals between GPS estimates of the clock 16–clock 21 difference and the difference measured using conventional hardware for b) pseudorange data and c) carrier-phase data. A mean has been subtracted from each time series. Note the difference in scales. The pseudorange RMS agreement is 2.38 ns. The carrier-phase RMS agreement is 0.55 ns.

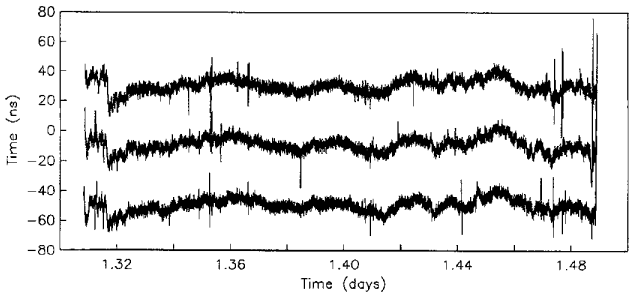

Fig. 5. Common view time-transfer estimates for a 2-m baseline at NIST using GPS satellite 9 on 3 consecutive days.

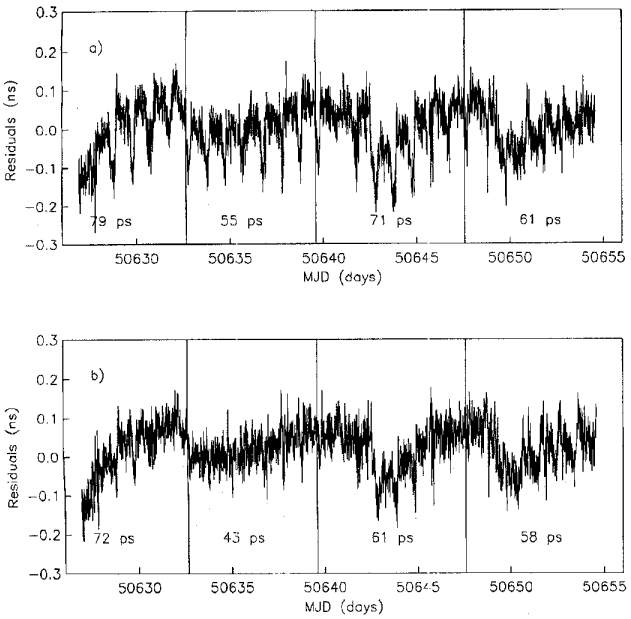

Fig. 6. a) Residual agreement between GPS carrier-phase measurements for NIST clock 16 and clock 21 and the local NIST measuring system after a mean has been subtracted from each time series. The vertical lines represent breaks in the data that occurred when the receiver connected to clock 21 lost lock on all satellites and reset its clock (see text for further discussion). The RMS is shown for each segment separately. b) The same estimates are shown with a multipath fit removed, as described in the text.

that GPS antennas on the roof of NIST have substantial multipath effects. To illustrate this, Fig. 5 shows the common view time difference between two code-based timing receivers connected to the same clock. The antennas of the two receivers were located on the roof of NIST and were separated by about 2 m. Each trace in the figure shows the common view time difference as a function of UTC time on consecutive days. Note the reproducibility of the structure in the time differences and the change in the character of the time difference as the satellite moves lower on the horizon. This plot shows only the differential effects of multipath. Differential multipath effects will increase with the distance between the two antennas but will be less important in carrier-phase estimates because the carrier-phase measurement is more precise than pseudorange measurements. Therefore, our observation of 50 to 100 ps time transfer in the carrier-phase estimates is consistent with our observations of 2 to 10 ns for pseudorange techniques.

In Fig. 6(a), we have plotted carrier-phase "truth" residuals for clock 16–clock 21 over a 28-d period. The vertical lines represent times when the receiver connected to clock 21 "reset" its clock. By comparison, the receiver connected to clock 16 never reset its clock during the 3 months we used it for time-transfer experiments. These resets occur in two circumstances: when the clock has drifted by more than 0.03 s or when the receiver has recorded a "clock set" command. The latter occurs when power has been turned off or when the receiver has lost track of several satellites, rendering it incapable of determining position. Because position is the primary output of a geodetic receiver, the receiver resets all parameters, including the clock, and searches the sky to reacquire all visible satellites. Because geodetic GPS receivers were designed to be used by surveyors and geophysicists, it was expected that the units would be used in the field on battery power. Thus, power is frequently turned off. For laboratory use and timing applications, power outages should be minimal. We are still investigating why these two receivers, produced by the same manufacturer, had different reset characteristics. When geodetic receivers are installed in a laboratory environment, the 1-pulse/s output can also be monitored. This output can be used to calibrate the resets; recent (unpublished) results suggest 5-ps precision. We did not monitor the 1-pulse/s output during the experiments described in this paper.

To test the periodicity of the residuals, we have taken the residuals from days 50,633 and 50,634 and fit these data with a low-order polynomial. Using a model consisting of that fit, along with a 4-min shift, we recomputed the clock 16–clock 21 residuals, which are shown in Fig. 6(b). The accuracy of all segments is improved, although other structures in the residuals remain. The rather abrupt changes in the residuals (near 50,642.5 and 50,649.0) are correlated with poor data quality from the receiver connected to clock 21—the receiver lost lock on several satellites at these times.

We repeated our experiment at the US Naval Observatory (USNO) to examine the carrier-phase method in another multipath environment. Using identical estimation procedures, we estimated the difference between two hydrogen masers, which we designate as clock 2 and clock 52. The GPS antennas were separated by 157 m and were also located on a roof environment. The USNO clocks are regularly monitored by the USNO timing system. The comparison between GPS estimates and the USNO timing system is shown in Fig. 7. Any multipath signature is significantly smaller than we observed at NIST. The RMS of the residuals to the "truth" measurement is 35 ps over 6 d, as compared with our best estimate of 55 ps over a similar period at NIST. These short baseline results are consistent with other reports [6]–[8].

In both the USNO and NIST short baseline experiments, we connected two GPS receivers/antennas to two clocks. The strong diurnal signal in the residuals at NIST suggests that the multipath environment was different at the two antennas. Although the diurnal signal at USNO is less apparent, there is clearly structure in the residuals, which is not white. The results might also be explained by a difference in the temperature sensitivities of the two antennas. Assuming that the diurnal variation is on the order of 5°C RMS, ascribing this effect to temperature fluctuations would imply a difference in the temperature sensitivities of about 10 ps/°C. A difference in the temperature sensitivities of this magnitude is unlikely but is not absolutely impossible.

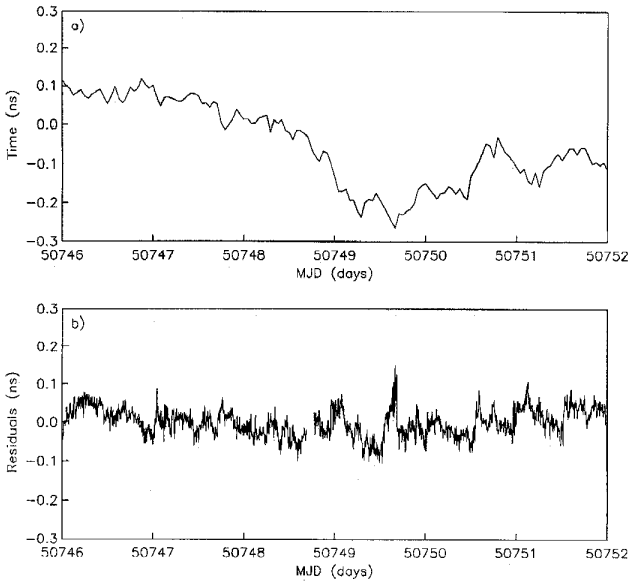

Fig. 7. Difference between clock 52 and clock 2 at the US Naval Observatory. a) Measured difference using the USNO timing system. b) Residual fit of the GPS carrier-phase estimates to series a. A mean has been subtracted from each time series. The RMS agreement is 35 ps.

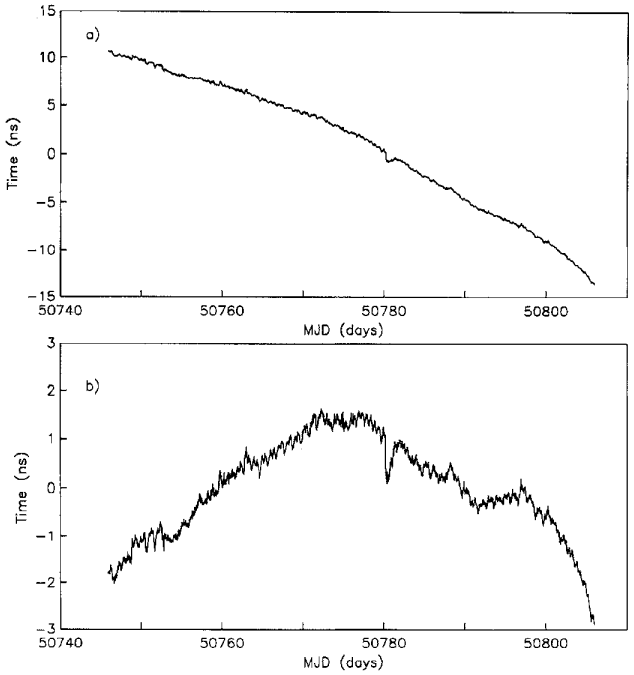

Fig. 8. a) GPS carrier-phase difference between NIST clock 16 and USNO clock 52; b) time series above, but detrended. A mean has been subtracted from each time series.

VI. Results for Long Baselines

Having established a lower bound on accuracy using GPS carrier phase at both USNO and NIST over short distances, we have extended our analysis to time transfer between USNO and NIST. Orbit errors, thermal effects, and atmospheric errors will no longer cancel at these distances, so we will have a more realistic assessment of the potential of GPS carrier phase for time transfer. Unfortunately, on long baselines, we are limited in our ability to define a truth standard. Time transfer between USNO and NIST is regularly monitored using two other techniques: GPS common view and two-way satellite time transfer (TWSTT). Common view time transfer can be conducted frequently but has a precision of only several nanoseconds. TWSTT systems are more precise than common view GPS techniques, but the measurements are expensive to make and are thus made infrequently. On the link between USNO and NIST, TWSTT measurements are made at most three times a week for periods of 5 min. The time stability for the TWSTT system is about 1 ns for τ of 1 day [29].

We analyzed the GPS carrier-phase data identically for USNO-NIST as we did for the short baseline, with the exception that we added data from Algonquin (Canada) and Goddard Space Flight Center for geodetic purposes. The station coordinates of Algonquin were tightly constrained to define the terrestrial reference frame properly. Goddard (24 km from USNO) was added to the analysis to help with ambiguity resolution.

To compare with TWSTT and common view, we first estimate the difference between NIST clock 16 and USNO clock 52. Clocks 16 and 52 are directly linked to dual frequency geodetic GPS receivers. Fig. 8(a) shows the difference between NIST clock 16 and USNO clock 52 for a 60-d period. The drift rate of the clock difference is 0.38 ns/d. There appear to be diurnal variations, although they are small compared with the overall trend. The detrended time series is shown in Fig. 8(b). In addition to long-term features and a diurnal signal, we also note a small transient offset of approximately 0.8 ns near MJD 50,780. This offset did not correlate with misfit in the GPS solution itself. Therefore, we looked at local clock records to determine whether the offset was due to local behavior at either NIST or USNO. We traced the offset to NIST clock 16.

In Fig. 9, we have plotted NIST clock 16 relative to three other hydrogen masers at NIST; a second-order polynomial is removed from each. The polynomial fit removes much of the frequency drifts among the four masers, allowing us to concentrate on the short-term structure. We also show the carrier-phase estimates between USNO and NIST clock 16; a second-order polynomial is removed. The carrier-phase time-transfer estimates are significantly noisier at periods of less than 1 d, but the longer-term structure is not significantly different than that observed in the local measurements.

In Fig. 10, we compare the time variance (TDEV) computed using the local measurements of NIST clock 30–NIST clock 16 with the USNO clock 52 to NIST clock 16 carrier-phase estimates. We did not fit a polynomial to either time series. These records demonstrate that the time-transfer noise is concentrated at periods of less than 1 d; the time stability is about 100 ps for averaging times of 1 d. The variance in the carrier-phase data at longer

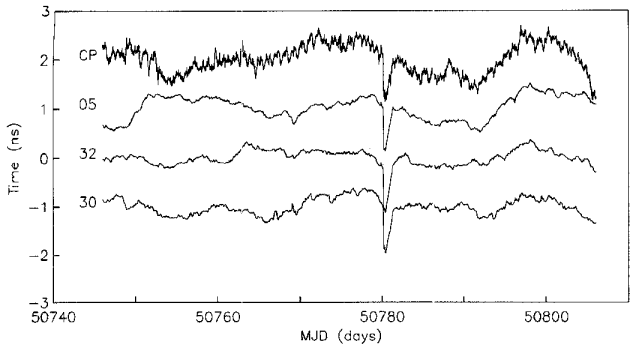

Fig. 9. NIST clocks 5, 32, and 30 relative to NIST clock 16. All four NIST clocks are hydrogen masers. A second-order polynomial has been removed from each differential clock record. Also shown are the carrier-phase (CP) estimates for USNO clock 52 to NIST clock 16, also with a second-order polynomial removed.

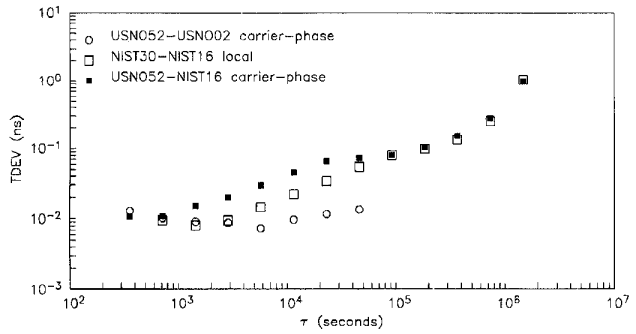

Fig. 10. TDEV calculation for USNO clock 52 to NIST clock 16 time series and NIST clock 30 relative to NIST clock 16. No polynomials were removed for either time series. Also shown are TDEV results for the short baseline test at USNO.

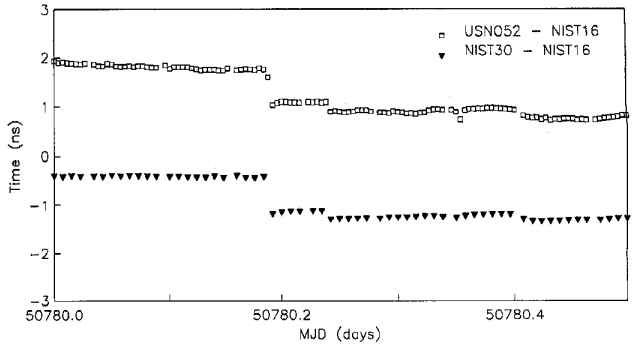

Fig. 11. Time transfer over a 12-hour period. The squares represent GPS estimates of time transfer (every 6 minutes) between NIST clock 16 and USNO clock 52. The inverted triangles (every 12 minutes) are local measurements between NIST clocks 16 and 30. The coincident measurements have an RMS agreement of 68 ps. The series are offset for display purposes only.

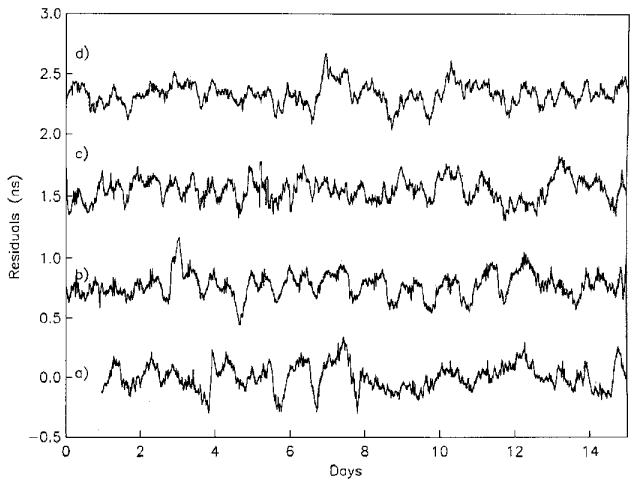

Fig. 12. GPS carrier-phase difference between NIST clock 16 and USNO clock 52, with low order polynomial and glitch removed, windowed in 15-d segments, for MJD a) 50745–5060, b) 50760–50775, c) 50775–50790, and d) 50790–50805. The RMS agreement over the 60-day segment is 93 ps.

times is consistent with the noise in the clocks themselves as observed using local measurements. For comparison, we also show the TDEV calculations for the short baseline results at USNO over a shorter period.

We can also examine the glitch at a higher resolution. In Fig. 11, we show the difference between NIST clock 16 and NIST clock 30 plotted with the GPS estimates for the USNO-NIST time series at MDJ 50,780. Even though we are using estimates from a 2400-km time-transfer experiment, the RMS residual agreement about the mean is 68 ps.

In Fig. 12, we replot the NIST-USNO time series without the long-term features and with the 50,780 offset removed. Although these residuals appear to have a diurnal signal, multipath is not the only contributor to the residuals. More likely, these residuals demonstrate the current limitations of GPS carrier-phase time transfer: multipath; temperature-related errors in the GPS antennas, receivers, and cables; errors in the models of the troposphere; and orbit errors. The RMS of the residuals shown in Fig. 12 is 93 ps.

We cannot directly compare the carrier-phase estimates with other measurement systems. First, we must apply corrections to connect USNO clock 52 and NIST clock 16 with the clocks used for the other measurement techniques. Fig. 13 shows that the local corrections can be significant. Once these corrections have been applied, we can compare the carrier-phase estimates with common view and TWSTT measurements for the same baseline. In Fig. 14(a), we show 30-min common view results. If we average the common-view values for 24 h [Fig. 14(b)], we can begin to see good correlation with the GPS carrier-phase analysis. In Fig. 14(c), we plot a comparison between GPS carrier phase and TWSTT. Good agreement between TWSTT and GPS carrier phase suggests that there is no long-term error in the carrier-phase time-transfer analysis.

We have also calculated the Allan deviation for the common view and carrier-phase estimates shown in Fig. 14. Frequency uncertainty for carrier-phase estimates is two

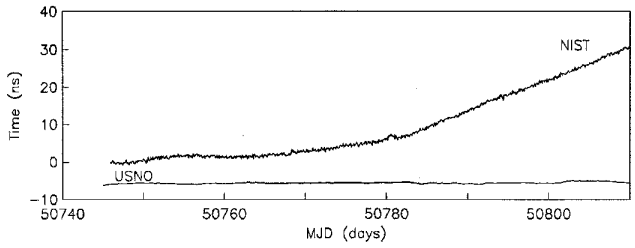

Fig. 13. Local UTC corrections for NIST clock 16 and USNO clock 52. These corrections must be used to compare the carrier-phase estimates with TWSTT and common view estimates between USNO and NIST.

parts in 10^{15} for an average time of 1 day, more than an order of magnitude better than can be achieved with the common view technique.

Figs. 10, 12, and 15 all suggest that there is significant noise in the carrier-phase time-transfer estimates at periods less than 1 d. Some of this could be due to thermal effects in the antennas, receivers, and cables. Careful studies on short baselines [9] have demonstrated that not only do GPS receiver delays depend on temperature, but receivers manufactured by the same company can have significantly different dependences on temperature. One was measured to have a dependence of 0.022 ns/°C, and the other had a nonlinear dependence on temperature. This suggests that each receiver must be calibrated or that each receiver must be operated in a stable thermal environment. The receivers used in this experiment were not calibrated, although they were kept in fairly stable temperature environments, with variations of less than 2°C/d.

The temperature dependence of the antenna is less clear, with reports as high as 0.1 ns/°C [9]. More recent studies suggest that the use of a temperature-stabilized antenna would be appropriate [30]. Finally, cable delays are known to vary depending on the dielectric constant of the cable [9]; values as high as −0.42 ps/°C-m have been reported. Given that differential temperature variations are as high as 10°C between Boulder, Colorado and Washington, D.C., one could produce large diurnal variations from the cables and/or antennas. The calibration of these thermal effects will be the subject of an upcoming paper.

Changes in the electrical parameters of the antenna cable are also likely to change the voltage standing-wave ratio (VSWR) at the connection to the receiver, and this may introduce additional temperature-dependent (and frequency-dependent) delays. The magnitude of this effect is a function of the mismatch in the impedance between the cable and its terminators, and these effects are likely to vary among nominally identical receivers. The VSWR can be measured using standard hardware, but many timing laboratories are not equipped to make these measurements on a routine basis.

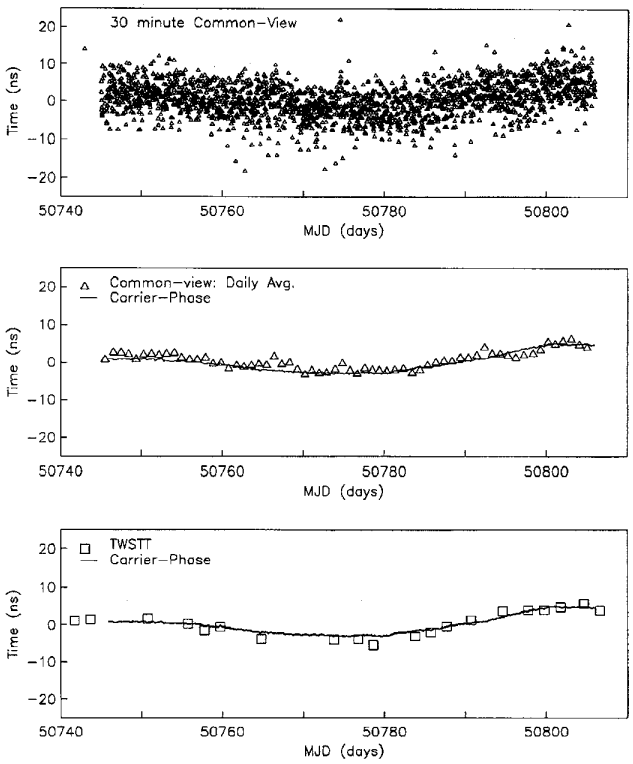

Fig. 14. Time transfer between USNO and NIST for a 60-day period after local UTC corrections have been applied. A mean has been subtracted from each time series. a) Thirty-minute common view estimates; b) daily average common view estimates compared with carrier-phase estimates; and c) TWSTT estimates compared with carrier-phase estimates.

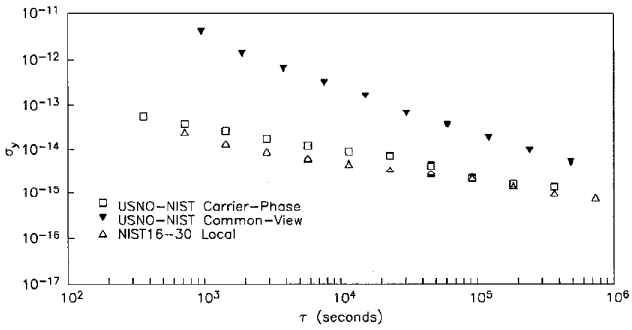

Fig. 15. Allan deviation for USNO-NIST carrier-phase estimates (with local UTC corrections) and 30-min common view estimates. For comparison, the Allan deviation for local clock measurements at NIST are also shown (clock 16 relative to clock 30).

VII. Discussion

These results confirm the resolution that can be realized by applying carrier-phase methods to time and frequency distribution. In the long run, however, the usefulness of the technique for frequency comparisons will depend on the stability of the delays and other systematic offsets in the hardware; to be useful for time distribution, these biases must be both stable and accurately known. It is not clear whether these requirements can be satisfied with existing receivers.

Previous studies have reported that the delay through the receiver is affected by temperature and similar effects [14]. Although these are important issues, they can be solved (or at least addressed) by appropriate choice of components. Our discussion is directed toward issues that arise from the nature of the phase measurement itself.

All hardware phase measurements are inherently ambiguous because the integer number of cycles cannot be determined as part of the measurement process. The process becomes more complicated in a GPS receiver because the local oscillator and the GPS carrier are at very different frequencies. The difference between these two frequencies is usually bridged in two steps—a fixed-frequency local oscillator that translates the carrier from L band to a much lower frequency using conventional mixers and a digital tracking loop that locks onto the heterodyned carrier from each satellite and deals with Doppler shifts and other offsets that are constant or vary relatively slowly with time.

This two-step process exploits the best aspects of analog and digital systems, but it introduces a fundamental ambiguity in the phase measurement process because the effective delay through the receiver is the sum of the offsets introduced by both procedures. Therefore, the first requirement for a carrier-phase receiver is that the output data accurately reflect this physical phase delay and not just the digital part of it. The simplest way of realizing this requirement is to ensure that the hardware component of the phase delay is a simple constant that must be determined only once during the calibration of the receiver. Earlier we mentioned the problem of clock resets and geodetic receivers. Although there have been some results that suggest the receiver itself can calibrate these resets with very high precision, this needs to be verified with a larger data set. It is not clear whether there are any receivers that currently satisfy these requirements; the receivers we have used to date do not do so consistently, at least in their normal operating configurations.

Time-transfer using carrier-phase data and geodetic estimation techniques is very promising. Much of the success shown in these initial studies is due to improvements made by the geodetic community, in particular, the development and maintenance of a high quality tracking network for determining precise GPS ephemerides. Model improvements for the troposphere are critical for time transfer and were originally pioneered for geodetic applications. However, there are parts of the time-transfer problem that have not been addressed by geodetic estimation techniques. To some extent, this is because of the difference between the statistics of the two types of observables. Most geodetic observations are analyzed in segments of 24 h. Variations with shorter periods have, for the most part, been ignored, at least partially, because the geodetic parameters are assumed to be constant (or at most linearly varying) over these time periods. Averaging over 24 h significantly attenuates many effects, including multipath reflections and thermally induced changes in the effective delay through the station hardware.

Unfortunately, such averaging periods may be too long for time-transfer measurements because the variance in time-transfer data may have significant contributions from flicker and random-walk phase-noise processes at periods of a few hours and longer. (This will be especially important if time steps or frequency steps in the station clocks are a problem.) The need to use shorter averaging times increases the importance of short-period fluctuations on time-transfer data relative to their effect on geodetic observations. In addition to the challenges inherent in finding or developing a geodetic GPS receiver that will meet the requirements discussed previously, it will also be necessary to study contributions to the variance with periods of less than a day to achieve the most accurate and precise carrier-phase time-transfer results.

VIII. Conclusions

Hydrogen masers at NIST and USNO were connected to off-the-shelf geodetic GPS receivers for a 60-d period. Carrier-phase and pseudorange data from these receivers were then analyzed using geodetic techniques. We have demonstrated time transfer with a stability of 100 ps and a frequency uncertainty of two parts in 10^{15} for an average time of 1 day. Carrier-phase time transfer is clearly significantly more precise than the GPS common view technique. The comparisons with TWSTT are very promising, although it would be beneficial to compare with more frequent TWSTT measurements. There remain several important areas for GPS carrier-phase time-transfer research: thermal sensitivities in antennas, cables, and receivers; troposphere modeling, multipath multigation; and orbit errors.

Acknowledgments

We thank Ed Manzanares, Ulf Lindquister, Tom Meehan, Demetrios Matsakis, Ed Powers and Jim Ray for lending us equipment, collecting data, and helpful discussions. We are particularly grateful to Tom Parker and Larry Young for comments on the manuscript. We acknowledge computing facilities funded by NASA grant NAG1908. The GIPSY software was written by the Jet Propulsion Laboratory, California Institute of Technology. We gratefully acknowledge the IGS for providing GPS ephemerides and

the IERS for polar motion and Earth orientation parameters.

REFERENCES

[1] D. Allan and M. Weiss, "Accurate time and frequency transfer during common-view of a GPS satellite," in *Proc. 1980 IEEE Freq. Contr. Symp.*, Philadelphia, PA, pp. 334–356.

[2] J. Levine, "Time transfer using multi-channel GPS receivers," in *Proc. IEEE 1998 Freq. Contr. Symp.*, Pasadena, CA, pp. 284–291.

[3] P. Segall and J. Davis, "GPS applications for geodynamics and earthquake studies," *Annu. Rev. Earth Planetary Sci.*, vol. 25, pp. 310–336, 1997.

[4] G. Blewitt, M. Heflin, W. Bertiger, F. Webb, U. Lindqwister, and R. Malla, "Global coordinates with centimeter accuracy in the international terrestrial reference frame using the Global Positioning System," *Geophys. Res. Lett.*, vol. 19, pp. 853–856, 1992.

[5] C. Dunn, D. Jefferson, S. Lichten, J. B. Thomas, and Y. Vigue, "Time and positioning accuracy using codeless GPS," in *Proc. 25th Precise Time and Time Interval Applicat. Planning Mtg.*, Marina Del Rey, CA, 1993, pp. 169–182.

[6] D. Jefferson, S. Lichten, and L. Young, "A test of precision GPS clock synchronization," in *Proc. 1996 IEEE Freq. Contr. Symp.*, Honolulu, HI, pp. 1206–1210.

[7] P. Baeriswyl, T. Schildknecht, J. Utzinger, and G. Beutler, "Frequency and time-transfer with geodetic GPS receivers: First results," in *Proc. 9th Eur. Freq. Time Forum*, Besanlon, France, 1995, pp. 46–51.

[8] P. Baeriswyl, T. Schildknecht, T. Springer, and G. Beutler, "Time-transfer with geodetic GPS receivers: Using code and phase observations," in *Proc. 10th Eur. Freq. Time Forum*, Neuchatel, Switzerland, 1996, pp. 430–435.

[9] F. Overney, T. Schildknecht, G. Beutler, L. Prost, and U. Feller, "Time-transfer with geodetic GPS receivers: Middle-term stability and temperature dependence of the signal delays," in *Proc. 11th Eur. Freq. Time Forum*, Besanlon, France, 1997, pp. 504–508.

[10] F. Overney, L. Prost, G. Dudle, T. Schildknecht, G. Beutler, J. Davis, J. Furlong, and P. Hetzel, "GPS time-transfer using geodetic receivers (GeTT): Results on European baselines," in *Proc. 12th Eur. Freq. Time Forum*, Milan, Italy, 1998.

[11] K. Larson and J. Levine, "Time-transfer using the phase of the GPS carrier," *IEEE Trans. Ultrason., Ferroelect., Freq. Contr.*, vol. 45, no. 3, pp. 539–540, 1998.

[12] ——, "Time-transfer using the phase of the GPS carrier," in *Proc. 1998 IEEE Freq. Contr. Symp.*, Pasadena, CA, pp. 292–297.

[13] B. Hofmann-Wellenhof, H. Lichtenegger, and J. Collins, *Global Positioning System: Theory and Practice*. New York: Springer-Verlag Wien, 1994.

[14] S. Lichten and J. Border, "Strategies for high-precision Global Positioning System orbit determination," *J. Geophys. Res.*, vol. 92, pp. 12,751–12,762, 1987.

[15] G. Bierman, *Factorization Methods for Discrete Sequential Estimation*. San Diego, CA: Academic, 1977.

[16] T. Herring, J. Davis, and I. Shapiro, "Geodesy by radio interferometry: The application of Kalman filtering to the analysis of very long baseline interferometry data," *J. Geophys. Res.*, vol. 95, pp. 12,561–12,581, 1990.

[17] K. Larson and D. Agnew, "Application of the Global Positioning System to crustal deformation measurement 1. Precision and accuracy," *J. Geophys. Res.*, vol. 96, pp. 16,547–16,566, 1991.

[18] Y. E. Bar-Sever, "A new model for GPS yaw attitude," in *Proc. IGS Workshop: Special Topics and New Directions*, G. Gendt and G. Dick, Eds. Potsdam, Germany: GeoForschungsZentrum, 1996, pp. 128–140.

[19] G. Beutler, I. I. Mueller, and R. E. Neilan, "The internation GPS service for geodynamics (IGS): Development and start of official service on January 1, 1994," *Bull. Geodesique*, vol. 68, no. 1, pp. 39–70, 1994.

[20] A. E. Niell, "Global mapping functions for the atmospheric delay at radio wavelengths," *J. Geophys. Res.*, vol. 101, pp. 3227–3246, 1996.

[21] J. Davis, "Atmospheric propagation effects on radio interferometry," Ph.D. dissertation, MIT, Cambridge, 1986.

[22] I. Saastamoinen, "Contribution to the theory of atmospheric refraction," *Bull. Geodesique*, vol. 107, pp. 13–34, 1973.

[23] Y. Bar-Sever, P. Kroger, and J. Borjesson, "Estimating horizontal gradients of tropospheric path delay with a single GPS receiver," *J. Geophys. Res.*, vol. 103, pp. 5019–5035, 1988.

[24] D. MacMillan, "Atmospheric gradients from very long baseline interferometry observations," *Geophys. Res. Lett.*, vol. 22, pp. 1041–1044, 1995.

[25] J. Davis, G. Elgered, A. Niell, and C. Kuehn, "Ground-based measurements of the gradients in the "wet" radio refractivity of air," *Radio Sci.*, vol. 28, pp. 1003–1018, 1993.

[26] G. Blewitt,"An automatic editing algorithm for GPS data," *Geophys. Res. Lett.*, vol. 17, pp. 199–202, 1990.

[27] ——, "Carrier-phase ambiguity resolution for the Global Positioning System applied to geodetic baselines up to 2000 km," *J. Geophys. Res.*, vol. 94, pp. 10,187–10,282, 1989.

[28] J. B. Thomas, "Signal-processing theory for the TurboRogue receiver," *JPL Publ.*, vol. 95-6, Apr. 1995.

[29] C. Hackman, S. Jefferts, and T. Parker, "Common-clock two-way satellite time-transfer experiments," in *Proc. 1995 IEEE Freq. Contr. Symp.*, San Francisco, CA, pp. 275–281.

[30] G. Petit, C. Thomas, and Z. Jiang, "Use of geodetic GPS Ashtech Z12T receivers for accurate time and frequency comparisons," in *Proc. 1998 IEEE Freq. Contr. Symp.*, Pasadena, CA, pp. 306–314.

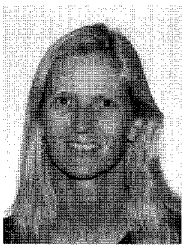

Kristine Larson was born in Santa Barbara, California in 1962. She received an A.B. degree in Engineering Sciences from Harvard University in 1985 and a Ph.D. in Geophysics from the Scripps Institution of Oceanography, University of California at San Diego in 1990. Her dissertation applied the Global Positioning System to measurements of tectonic motion in the offshore regions of southern California.

From 1988 to 1990, Dr. Larson was also a member of the technical staff of the radiometric tracking division at the Jet Propulsion Laboratory. Since 1990, she has been a faculty member in the Department of Aerospace Engineering Sciences at the University of Colorado at Boulder where she is currently an associate professor. The primary focus of her work is system development of the GPS and applications to measuring plate tectonics, ice flow, plate boundary deformation, volcanic activity, ice mass balance, and time transfer.

Dr. Larson is a member of the American Geophysical Union.

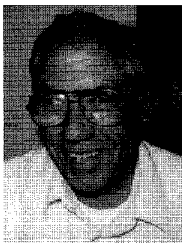

Judah Levine was born in New York City in 1940. He received a Ph.D. degree in Physics from New York University in 1966. He is currently a physicist in the Time and Frequency Division of the National Institute of Standards and Technology (NIST) in Boulder, Colorado and is also a Fellow of the Joint Institute for Laboratory Astrophysics, which is operated jointly by NIST and the University of Colorado at Boulder.

He is currently studying new methods for distributing time and frequency information using digital networks, such as the Internet, and on ways of improving satellite-based time and frequency distribution.

Dr. Levine is a Fellow of the American Physical Society and is a member of the American Geophysical Union and the IEEE Computer Society.